JACS
JOURNAL OF THE AMERICAN CHEMICAL SOCIETY
Communication
pubs.acs.org/JACS

Supramolecular Photoactivatable Anticancer Hydrogels

V. Venkatesh,[†] Narendra Kumar Mishra,[‡] Isolda Romero-Canelón,[†] Robbin R. Vernooij,[†] Huayun Shi,[†] James P. C. Coverdale,[†] Abraha Habtemariam,[†] Sandeep Verma,[‡] and Peter J. Sadler*[,†]

[†]Department of Chemistry, University of Warwick, Gibbet Hill Road, Coventry CV4 7AL, United Kingdom

[‡]Department of Chemistry and Center for Nanoscience and Soft Nanotechnology, Indian Institute of Technology Kanpur, Kanpur 208016, Uttar Pradesh, India

Supporting Information

ABSTRACT: A photoactivatable dopamine-conjugated platinum(IV) anticancer complex (**Pt-DA**) has been incorporated into G-quadruplex G_4K^+ borate hydrogels by using borate ester linkages (**Pt-G_4K^+B** hydrogel). These were characterized by ^{11}B NMR, attenuated total reflection Fourier transform infrared spectroscopy, circular dichroism, scanning electron microscopy and transmission electron microscopy. Microscopy investigations revealed the transformation of an extended fiber assembly into discrete flakes after incorporation of **Pt-DA**. **Pt-DA** showed photocytotoxicity against cisplatin-resistant A2780Cis human ovarian cancer cells (IC_{50} 74 μM, blue light) with a photocytotoxic index <2, whereas **Pt-G_4K^+B** hydrogels exhibited more potent photocytotoxicity (IC_{50} 3 μM, blue light) with a photocytotoxic index >5. Most notably, **Pt-DA** and **Pt-G_4K^+B** hydrogels show selective phototoxicity for cancer cells versus normal fibroblast cells (MRC5).

Although hydrogels are mostly water, they behave like solids due to three-dimensional networks of cross-links within them. Hydrogels often consist of cross-linked polymers and have the properties of colloidal particles.[1] The cross-linking can be stabilized by many kinds of interactions such as van der Waals and covalent interactions, and hydrogen bonding.[2] There is increasing interest in designing hydrogels made from biomolecules with potential applications in biology, medicine and materials science. Stimuli-responsive hydrogels are particularly attractive in the field of drug delivery and tissue engineering.[3] Guanosine monophosphate (5′-GMP) and other derivatives of guanosine have been known to form gels for decades.[4] Guanosine-based hydrogels are stabilized by stacking of G-quartets on top of one another to form extended helices. Recently, Davis et al. designed G_4K^+ borate hydrogels and studied the role of the anion and cation in the stability of the gels.[5] They noted that when the guanosine analogue acyclovir, an antiviral drug, is incorporated in to the G_4K^+ borate hydrogel, the release of acyclovir is facilitated by the slow self-destruction of the hydrogel. This strategy can be successfully applied to provide slow and sustained release of acyclovir from G_4K^+ borate hydrogels.[6]

Flexibility and high water content of hydrogels allow them to mimic natural tissues, thereby paving the way for the development of hydrogel-based delivery systems particularly for topical medication. Recently, injectable hydrogels have been shown to have potential as delivery vehicles for cancer therapy.[7] Photochemotherapy for cancer has the potential to provide spatial and temporal control of drug activity in tumors with fewer side-effects on normal cells, as well as novel mechanisms of action which combat resistance. The anticancer activity of diazido-Pt(IV) complexes is mainly due to photoreduction of inert Pt(IV) to cytotoxic Pt(II) together with release of reactive azidyl radicals.[8] Small molecule cancer drugs often suffer from systemic toxicity and lack of selective uptake by cancer cells. The incorporation of photoactive platinum-based anticancer drugs in hydrogels limits drug exposure and facilitates slow release of the drug specifically at the target site, triggered by light irradiation.

Here we use biocompatible G_4K^+ hydrogels to deliver a photoactivatable a platinum(IV) prodrug to cancer cells. This strategy might allow treatment of surface cancers such as esophagus, lung, skin and bladder using spatially directed irradiation with minimal damage to normal tissues. To achieve this goal, we have synthesized a photoactivatable diazido-Pt(IV) complex appended with dopamine, a neurotransmitter as well as a constituent of adhesive proteins in mussels. Dopamine and polydopamines possess self-assembly properties, extensively used as anchors for attachment of functional molecules on different substrates.[9] Moreover, the antiangiogenesis properties of dopamine have been explored by Basu et al.[10] We prepared a dopamine-conjugated photoactivatable Pt(IV) complex (**Pt-DA**) in order to conjugate it to a G_4K^+ borate hydrogel using catechol-borate and guanosine-borate interactions. The synthesis of **Pt-DA** involved reacting dopamine hydrochloride with *trans,trans,trans*-$[Pt(N_3)_2(Py)_2(OH)(succinate)]$ using amide coupling (Scheme S1). The photoactivation and decomposition of **Pt-DA** were investigated by irradiation with 420 nm blue light in 1:1 (v/v) methanol:water. The photoreaction was followed by UV−vis and ^1H NMR spectroscopy. The change in the UV−vis spectrum was monitored every 5 min for 1 h. Figure 2A shows the gradual reduction in intensity of the $N_3\rightarrow$ Pt LMCT band at ca. 300 nm corresponding to electron transfer from azide to Pt(IV) and formation of Pt(II). To understand the reduction process, ^1H NMR spectra of **Pt-DA** in the dark were recorded as well as after irradiation at 420 nm for 2 h. The ^1H NMR spectrum showed the presence of both Pt(II) and Pt(IV) species (Figure 2B). The UV−vis spectrum showed the formation of a broad band around 420−600 nm after irradiation,

Received: January 6, 2017
Published: April 17, 2017

DOI: 10.1021/jacs.7b00186
J. Am. Chem. Soc. 2017, 139, 5656−5659

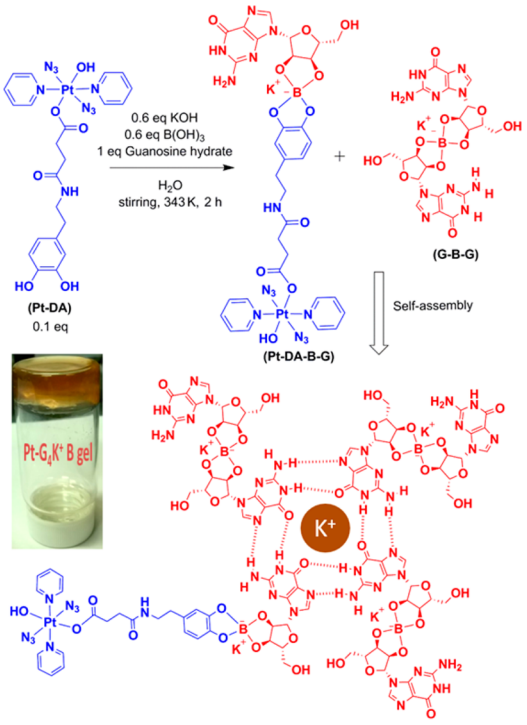

Figure 1. Schematic representation of the self-assembly of **Pt-DA** functionalized G_4K^+ borate hydrogels. (Inset shows synthesized **Pt-G_4K^+B** hydrogel.)

indicating slow oxidation of dopamine to the quinone. **Pt-G_4K^+B** hydrogel was prepared in a one-pot reaction by treating **Pt-DA** with boric acid and potassium hydroxide in water for 30 min, followed by the addition of guanosine hydrate, under constant stirring for 2 h at 343 K (Scheme S2). The reaction mixture was then allowed to cool to ambient temperature overnight affording a brown-colored gel (Figure 1 inset).

To investigate how **Pt-DA** is attached to G_4K^+ borate hydrogel, we treated **Pt-DA** with boric acid and potassium hydroxide (without guanosine hydrate) yielding **Pt-DA**-borate ester (**Pt-DA-B**). **Pt-DA** is sparingly soluble in water, but after mono borate ester formation the solubility improved. A color change from yellow to dark brown was observed within a few minutes, indicating formation of the monoborate ester. The progress of the reaction was monitored by UV−vis spectroscopy, which showed the appearance of a weak band at ca. 400−550 nm corresponding to monoborate ester, similar to that reported by Kim et al. during catechol-borate gel formation.[11] ^{1}H NMR showed the disappearance of catechol −OH resonances at 8.62 and 8.73 ppm after mono borate ester formation. This was further confirmed by electrospray ionisation mass spectrometry (ESI-MS, Figure S3). This observation clearly indicated that the brown color of the gel is due to the incorporation of **Pt-DA-Borate** ester, whereas G_4K^+ borate hydrogel is colorless. The mol ratio of **Pt-DA** relative to guanosine hydrate is crucial for gel formation, when 1 mol equiv of **Pt-DA** was used, no gel formation was observed. The presence of the **Pt-DA** functional group on the four arms of the G-quartet may cause steric disruption to the stacking of G-quartets. Reducing the molar ratio of **Pt-DA** to 0.1 mol equiv resulted in gel formation.

The **Pt-G_4K^+B** hydrogel was characterized by attenuated total reflection Fourier transform infrared spectroscopy (ATR-FTIR) and ^{11}B NMR. ATR-FTIR spectra of **Pt-G_4K^+B** hydrogel, G_4K^+ borate hydrogel, guanosine and boric acid are shown in Figure 2D together with selected peak assignments. The amide vibration (ν(CO), δ(NH_2)) of free guanosine at 1726 cm^{-1}

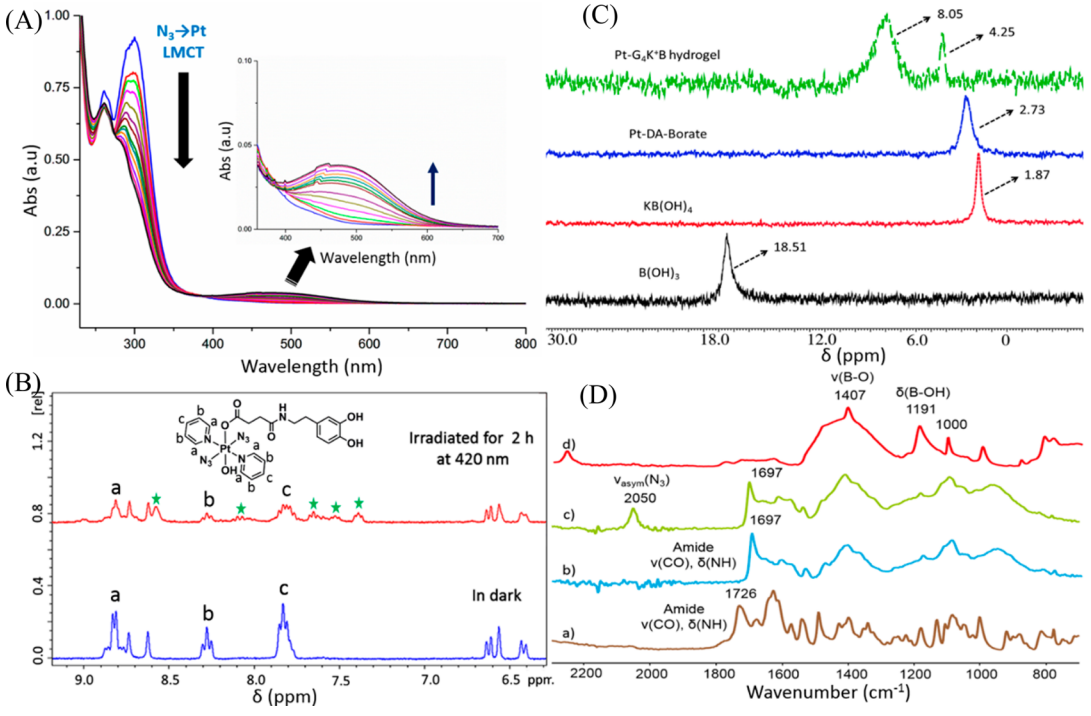

Figure 2. (A) UV−vis spectra of **Pt-DA** before and after irradiation with 420 nm blue light, scans were recorded every 5 min for 1 h in 1:1 v/v water: methanol. (B) ^{1}H NMR spectra of **Pt-DA** before and after irradiation at 420 nm in DMSO-d_6 (assignments: a, b, c correspond to Pt-py peaks, green colored stars correspond to Pt(II) photoproduct). (C) ^{11} B NMR spectra of boric acid, borate, **Pt-DA-Borate** and **Pt-G_4K^+B** hydrogel in D_2O. (D) ATR-FTIR spectra of (a−d) guanosine hydrate, **G_4K^+** borate hydrogel, **Pt-G_4K^+B** hydrogel and boric acid, respectively.

DOI: 10.1021/jacs.7b00186
J. Am. Chem. Soc. 2017, 139, 5656−5659

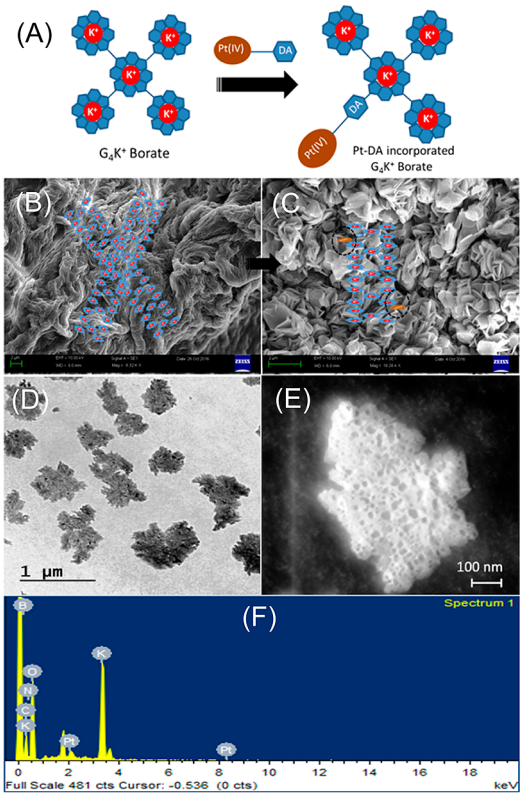

Figure 3. (A) Schematic representation of incorporation of **Pt-DA** into G_4K^+ borate hydrogel. (B and C) SEM images of G_4K^+ borate hydrogel and **Pt-G$_4$K$^+$B** hydrogel. (D) TEM image of **Pt-G$_4$K$^+$B** hydrogel. (E) STEM image shows the presence of pores in the flake assembly. (F) EDX of **Pt-G$_4$K$^+$B** hydrogel showing the elemental composition (K, Pt, C, N and O) of the flakes.

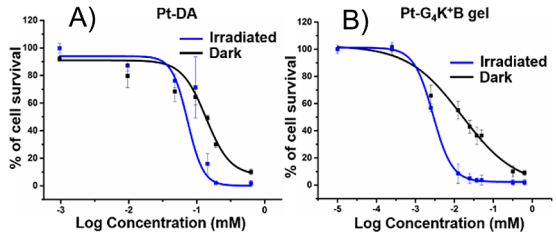

Figure 4. Growth curves for A2780Cis cells treated for 1 h with (A) **Pt-DA** and (B) **Pt-G$_4$K$^+$B** hydrogel, followed by 1 h irradiation with blue LEDs (465 nm, 50 mW). Cells were allowed to recover for 24 h in drug-free medium before determination of viability.

decreases in wavenumbers when guanosine amide is involved in H-bonding networks. As expected, the amide vibrations of **Pt-G$_4$K$^+$B** hydrogel, and G_4K^+ borate hydrogel appear at 1697 cm^{-1}. The observed decrease between guanosine and the gels (29 cm^{-1}) is due to intermolecular H-bonding between guanosines.[12] **Pt-G$_4$K$^+$B** hydrogel shows the $\nu_{asym}(N_3)$ at 2050 cm^{-1}, confirming the presence of **Pt-DA** (Figure S4). Boric acid (Figure 2**Dd**) gives rise to two δ(B−OH) vibrations at 1000 and 1191 cm^{-1}, and a broad ν(B−O) vibration at 1407 cm^{-1}. ATR-FTIR spectra of **Pt-G$_4$K$^+$B** hydrogel and G_4K^+ borate hydrogel show a broad feature for ν(B−O), whereas ν(B−OH) vibrations were not observed indicating the formation of borate diesters. Borate monoester and diester formation in D_2O were studied by ^{11}B NMR spectroscopy (Figure 2C). Boric acid shows a signal at 18.5 ppm, whereas borate displays a peak at 1.87 ppm. When **Pt-DA** was added, the latter signal shifted to 2.73 ppm indicating the formation of Pt-DA-monoborate ester (**Pt-DA-B**). Guanosine hydrate was then added to the solution, which was heated to 343 K for 2 h. The ^{11}B NMR spectrum showed two peaks at 4.25 and 8.05 ppm.

Table 1. IC_{50} (μM) Values for Pt-DA and Pt-G$_4$K$^+$ Borate Hydrogel against Cisplatin-Resistant A2780Cis Human Ovarian Cancer Cells and normal MRC-5 Human Fibroblast Cells, in Comparison with Chlorpromazine (CPZ) and Cisplatin (CDDP)[a]

	IC_{50} (μM)			
	A2780Cis		MRC5	
compound	dark	blue (465 nm)	dark	blue (465 nm)
Pt-G$_4$K$^+$B gel	15.8 ± 0.6	2.8 ± 0.3	>50	>50
Pt-DA	138.03 ± 0.09	74.1 ± 0.2	>200	>150
CPZ	51.2 ± 0.4	6.3 ± 0.2	>100	>50
CDDP	>100	>100	>100	>100

[a]CDDP is nontoxic under the short treatment conditions used here (1 h drug exposure). IC_{50} values for **Pt-DA**, **Pt-G$_4$K$^+$** and CDDP (concentration for 50% cell growth inhibition), based on Pt concentrations by ICP-OES.

The peak at 4.25 ppm corresponds to borate diester of Pt-DA and guanosine (**Pt-DA-B-G**) and the peak at 8.05 ppm to guanosine borate diester (**G-B-G**).

The **Pt-G$_4$K$^+$B** hydrogel was also characterized by microscopy. Scanning electron microscopy (SEM) images of the **Pt-G$_4$K$^+$B** gel in water show flake-like assemblies (Figure 3C). Further the Energy Dispersive X-ray (EDX) spectrum of **Pt-G$_4$K$^+$B** gel confirmed the presence of C, O, N, B, K and Pt in the flakes (Figure 3F). As a control, the self-assembly of G_4K^+ borate hydrogel was studied under similar conditions as those for **Pt-G$_4$K$^+$B** gel. G_4K^+ borate hydrogel forms an extensive fiber assembly due to stacking of G-quartets in helices (Figure 3B), an observation which matches well with a recent report.[5a] Transmission electron microscopy (TEM) images also show flake-like assembly (Figure 3D). We also performed raster scanning transmission electron microscopy (STEM) for better spatial resolution. STEM images indicate the presence of pores in the flakes (Figure 3E), suggesting that incorporation of **Pt-DA** has a significant role in the transformation of extensive fibril assembly into discrete flakes.

We recorded circular dichroism (CD) spectra to characterize changes in conformation that might accompany changes in the assembly process (Figure S5). The CD spectrum of G_4K^+ borate hydrogel shows two positive peaks at 254 and 295 nm and a negative peak at 234 nm. This CD spectrum confirms the formation of G_4 quartet stacking in the G_4K^+ borate hydrogel.[5a] Stacking occurs in both head-to-head and head-to-tail fashion. After addition of **Pt-DA**, significant changes were observed in the CD spectrum of **Pt-G$_4$K$^+$B** gel. This observation supports the conclusion that incorporating **Pt-DA** affects the conformation and hence the assembly process.

The anticancer activity of **Pt-DA** and **Pt-G$_4$K$^+$B** hydrogel was determined in the dark as well as under blue light irradition, by using the sulforhodamine B (SRB) colorimetric assay. IC_{50} values were determined for cisplatin-resistant A2780Cis human ovarian cancer cells (Figure 4) and the noncancerous human fibroblast cell line MRC-5. Both cell lines were treated with **Pt-DA** and **Pt-G$_4$K$^+$B** hydrogel for 1 h in the dark, followed by irradiating one set of plates for 1 h using blue LEDs (465 nm, 50 mW), whereas the other was kept in a dark incubator. After

DOI: 10.1021/jacs.7b00186
J. Am. Chem. Soc. 2017, 139, 5656−5659

irradiation, the cells were allowed to recover over 24 h and compared with untreated cells that were irradiated under similar conditions. These experiments also compared irradiated versus nonirradiated untreated cells in order to confirm that the observed cell death was not the result of light exposure. The difference between these two cell populations was in no case statistically significant. **Pt-DA** was relatively nontoxic toward A2780Cis cells in the dark (IC_{50} 138 μM, Table 1), but upon irradiation with blue light it exhibited moderate antiproliferative activity (IC_{50} 74 μM, photocytotoxicity index (PI) 1.9). In contrast, **Pt-G_4K^+B** hydrogel displayed activity against A2780Cis in the dark (IC_{50} = 16 μM), and was highly potent upon irradiation (IC_{50} = 3 μM, Table 1) with a higher photocytotoxicity index (PI) of 5.6. Hence, both the photocytotoxicity and PI of **Pt-DA** increase significantly after incorporation into the G_4K^+ borate gel. We further investigated the survival of A2780Cis cells exposed to a mixture of (a) **Pt-DA** with borate in a molar ratio 1:6, and (b) **Pt-DA** with borate and guanosine in a molar ratio of 1:6:10. Remarkably, there were no statistical differences in survival of cells treated only with **Pt-DA** and those treated with mixtures a or b. Thus, neither borate nor guanosine increase the toxicity of **Pt-DA** per se, and hence the increase in potency of **Pt-G_4K^+B** compared to **Pt-DA** is related to the gel and the delivery (Figures S6 and S7). Our experiments also included controls in which A2780Cis cells were treated only with either borate (up to 1.5 mM) or guanosine (up to 2.5 mM), or a combination of both. In all three cases, the percentages of cell survival were not statistically different from those of untreated A2780Cis cells. To study their cell selectivity, we tested them against MRC-5 normal lung fibroblasts. Under the same experimental conditions, both **Pt-DA** and **Pt-G_4K^+B** hydrogel were nontoxic toward normal cells (IC_{50} > 50 μM) giving a photocytotoxicity selectivity factor (ratio of the activity between normal and cancer cells), of >18 for the **Pt-G_4K^+B** hydrogel.

In conclusion, we have used a new strategy to design hydrogels that can deliver photoactivatable Pt(IV) anticancer complexes to cancer cells. We conjugated a photoactive Pt(IV) complex to **G_4K^+B** hydrogel using borate ester formation. This modification transformed the self-assembled **G_4K^+B** hydrogel from extended fibers into discrete flakes. Incorporation of **Pt-DA** into the **G_4K^+B** hydrogel dramatically increased its photocytotoxic potency toward cisplatin-resistant human ovarian cancer cells. Most importantly, the chemical modification dramatically increased the selectivity between normal and cancer cells (>18-fold) which is an early indication of the possibility of reducing unwanted side effects by the use of the hydrogel as a delivery strategy. Such high potency and selectivity provides a strong basis for development of this new class of materials as photochemotherapeutic agents, with potential for localized immunogenic treatment of cancers.[13]

■ ASSOCIATED CONTENT

Supporting Information

The Supporting Information is available free of charge on the ACS Publications website at DOI: 10.1021/jacs.7b00186.

Syntheses, characterizations and additional experimental details (SEM, TEM, CD, ICP-OES, cell culture, antiproliferative assays), Schemes S1 and S2 (synthesis), Figures S1−S5 (NMR, ESI-MS, UV−vis, ATR-FTIR and CD) (PDF)

■ AUTHOR INFORMATION

Corresponding Author

*P.J.Sadler@warwick.ac.uk

ORCID

Sandeep Verma: 0000-0002-2478-8109

Peter J. Sadler: 0000-0001-9160-1941

Notes

The authors declare no competing financial interest.

■ ACKNOWLEDGMENTS

We thank the EPSRC (grant no. EP/G006792), The Royal Society (Newton International Fellowship for V.V.), University of Warwick (Chancellor's Scholarship for H.S. and WCPRS award for J.P.C.C.), the Monash-Warwick Alliance (R.R.V.), Bruker Daltonics (studentship for J.P.C.C.) for support and members of COST Action CM1105 for stimulating discussions. S.V. thanks JC Bose Fellowship for support and Advance Imaging Center, IIT Kanpur, for microscopy studies. We also thank Dr Lijiang Song and Philip Aston for assistance with mass spectrometry.

■ REFERENCES

(1) (a) Utech, S.; Boccaccini, A. R. *J. Mater. Sci.* **2016**, *51*, 271−310. (b) Weiss, R. G. *J. Am. Chem. Soc.* **2014**, *136*, 7519−7530.

(2) (a) Babu, S. S.; Praveen, V. K.; Ajayaghosh, A. *Chem. Rev.* **2014**, *114*, 1973−2129. (b) Steed, J. W. *Chem. Soc. Rev.* **2010**, *39*, 3686−3699.

(3) (a) Vashist, A.; Vashist, A.; Gupta, Y. K.; Ahmad, S. *J. Mater. Chem. B* **2014**, *2*, 147−166.

(4) (a) Gellert, M.; Lipsett, M. N.; Davies, D. R. *Proc. Natl. Acad. Sci. U. S. A.* **1962**, *48*, 2013−2018. (b) Bang, I. *Biochem. Z.* **1910**, *26*, 293−311. (c) Sreenivasachary, N.; Lehn, J.-M. *Proc. Natl. Acad. Sci. U. S. A.* **2005**, *102*, 5938−5943.

(5) (a) Peters, G. M.; Skala, L. P.; Plank, T. N.; Hyman, B. J.; Reddy, G. N. M.; Marsh, A.; Brown, S. P.; Davis, J. T. *J. Am. Chem. Soc.* **2014**, *136*, 12596−12599. (b) Peters, G. M.; Skala, L. P.; Plank, T. N.; Oh, H.; Reddy, G. N. M.; Marsh, A.; Brown, S. P.; Raghavan, S. R.; Davis, J. T. *J. Am. Chem. Soc.* **2015**, *137*, 5819−5827.

(6) Plank, T. N.; Davis, J. T. *Chem. Commun.* **2016**, *52*, 5037−5040.

(7) (a) Liu, Y.; Xiao, L.; Joo, K.-I.; Hu, B.; Fang, J.; Wang, P. *Biomacromolecules* **2014**, *15*, 3836−3845. (b) Shen, W.; Luan, J.; Cao, L.; Sun, J.; Yu, L.; Ding, J. *Biomacromolecules* **2015**, *16*, 105−115.

(8) Sokolov, A. Y.; Schaefer, H. F., III *Dalton Trans.* **2011**, *40*, 7571−7582.

(9) (a) Liu, Y.; Ai, K.; Liu, J.; Deng, M.; He, Y.; Lu, L. *Adv. Mater.* **2013**, *25*, 1353−1359. (b) He, T.; Shi, Z. L.; Fang, N.; Neoh, K. G.; Kang, E. T.; Chan, V. *Biomaterials* **2009**, *30*, 317−326. (c) Guardingo, M.; Bellido, E.; Miralles-Llumà, R.; Faraudo, J.; Sedó, J.; Tatay, S.; Verdaguer, A.; Busqué, F.; Ruiz-Molina, D. *Small* **2014**, *10*, 1594−1602. (d) Hong, S.; Yang, K.; Kang, B.; Lee, C.; Song, I. T.; Byun, E.; Park, K. I.; Cho, S.-W.; Lee, H. *Adv. Funct. Mater.* **2013**, *23*, 1774−1780. (e) Li, H.; Jia, Y.; Wang, A.; Cui, W.; Ma, H.; Feng, X.; Li, J. *Chem. - Eur. J.* **2014**, *20*, 499−504.

(10) (a) Basu, S.; Nagy, J. A.; Pal, S.; Vasile, E.; Eckelhoefer, I. A.; Bliss, V. S.; Manseau, E. J.; Dasgupta, P. S.; Dvorak, H. F.; Mukhopadhyay, D. *Nat. Med.* **2001**, *7*, 569−574. (b) Chakroborty, D.; Sarkar, C.; Mitra, R. B.; Banerjee, S.; Dasgupta, P. S.; Basu, S. *Clin. Cancer Res.* **2004**, *10*, 4349−4356.

(11) Wang, B.; Jeon, Y. S.; Park, H. S.; Kim, Y. J.; Kim, J.-H. *eXPRESS Polym. Lett.* **2015**, *9*, 799−808.

(12) Meng, L.; Liu, K.; Mo, S.; Mao, Y.; Yi, T. *Org. Biomol. Chem.* **2013**, *11*, 1525−1532.

(13) Agostinis, P.; Berg, K.; Cengel, K.; Foster, T. H.; Girotti, A. W.; Gollnick, S. O.; Hahn, S. M.; Hamblin, M. R.; Juzeniene, A.; Kessel, D.; Korbelik, M.; Moan, J.; Mroz, P.; Nowis, D.; Piette, J.; Wilson, B. C.; Golab, J. *Ca-Cancer J. Clin.* **2011**, *61*, 250−281.

DOI: 10.1021/jacs.7b00186
J. Am. Chem. Soc. 2017, 139, 5656−5659